DNA binding and cytotoxicity of copper (II) imidazole terpyridine complexes: Role of oxyanion, hydrogen bonding and π–π Interaction

ARTICLE *in* EUROPEAN JOURNAL OF MEDICINAL CHEMISTRY · AUGUST 2013

Impact Factor: 3.45 · DOI: 10.1016/j.ejmech.2013.07.051 · Source: PubMed

2 AUTHORS:

Dr.Manikandamathavan V M

11 PUBLICATIONS **62** CITATIONS

SEE PROFILE

Balachandran Unni Nair

Central Leather Research Institute

368 PUBLICATIONS **6,018** CITATIONS

SEE PROFILE

European Journal of Medicinal Chemistry 68 (2013) 244–252

Contents lists available at ScienceDirect

European Journal of Medicinal Chemistry

journal homepage: http://www.elsevier.com/locate/ejmech

Original article

DNA binding and cytotoxicity of copper (II) imidazole terpyridine complexes: Role of oxyanion, hydrogen bonding and π–π interaction☆

Verasundharam Manickavasagar Manikandamathavan, Balachandran Unni Nair*

Chemical Laboratory, Central Leather Research Institute, Council of Scientific Industrial Research, Adyar, Chennai 600 020, India

ARTICLE INFO

Article history:
Received 15 May 2013
Received in revised form
8 July 2013
Accepted 13 July 2013
Available online 14 August 2013

Keywords:
Antiproliferative activity
Copper (II) complexes
Cytotoxicity
DNA binding

ABSTRACT

Mononuclear complexes [Cu(Itpy)X(H_2O)]X (Itpy – imidazole terpyridine, X – NO_3 **1** and X – ClO_4 **2**) have been synthesized and characterized. Single crystal X-ray diffraction of complex **1** shows distorted octahedral geometry around the copper (II) ion. Presence of multiple hydrogen bonding network in the molecule results in anti-parallel stacking of the molecule. Both the complexes show dual mode of binding to DNA. Both the complexes have been found to bring about DNA cleavage in the presence of H_2O_2 and show potent cytotoxicity towards lung carcinoma cell line. The ability of the two complexes to induce apoptosis has been investigated by using combination of nuclear stains. FACS analysis shows that both the complexes bring about cell cycle arrest at 2.5 μM concentration.

1. Introduction

The accidental invention of cis-platin is one of the hallmarks for cancer chemotherapy [1–3]. Pursuing this footmark, derivatives of platinum complexes and many transition metal complexes were widely studied for cancer therapy [4–6]. DNA is the ultimate central target for most of the chemotherapeutic agents, either it may repair the DNA function or it will lead to apoptotic cell death, in order to control the proliferation. Considering the DNA as a target, drug molecule can interact through several binding modes broadly classified as covalent and non-covalent modes and further sub-classified as groove and intercalative modes etc. [7]. DNA binding mode of a metal complex is largely determined by the coordinated ligand. Among the metal ion based drugs, copper (II) complexes have attracted special attention due to the bio-essential nature of Cu (II) ion [8]. Terpyridine based copper (II) complexes have gained prominence because of the fact that the chelating ability of terpyridine enhances the stability of the complex, planarity of the ligand leads to strong intercalative interaction of the complex with DNA and then central metal acts as an anchor as well as reactive agent.

DNA is a classical bio molecule with well-defined grooves, electro negative backbone and helicity [9,10]. Similarly metal complexes have their own characteristic geometrical patterns. The interaction between the metal complex and DNA will be effective, when collision takes place between properly oriented drug molecules with DNA. Since, the interactions are in solution phase one cannot ignore the role of solvent molecule and non-covalent interactions. Coordinated ligands also play key role towards the binding of the metal complex to DNA targets like sugar, base and phosphate backbone [11]. Multiple mode of DNA binding can be achieved by having different types of ligands coordinated to the same metal centre. Chelating planar ligands coordinated to the metal ion can stack in between DNA bases and if the metal complex has additional monodentate anionic ligand, it can exchange with DNA base or phosphate directly. Such anionic ligands can also be involved in direct or water mediated hydrogen bonding with the DNA base or phosphate backbone. The effects of ionic strength, pH, geometry and planarity of the chelating ligand, on the interaction of metal complexes with DNA have been studied widely [12–15]. On the other hand; there are only limited reports on the effect of non-covalent forces like π–π interaction [16], H-bonding [17] and counter ion interaction [18] on the interaction of metal complexes with DNA.

In the present work, we describe the role of oxy anion and non-covalent forces like hydrogen bonding, π–π interaction of the co-ordinated ligand on the metal complex-DNA interactions, their nuclease activity and cytotoxicity.

☆ CCDC reference number: 926753.

* Corresponding author. Tel.: +91 44 24411630; fax: +9144 24911589.
E-mail addresses: bunair@clri.res.in, bunninair@gmail.com (B. Unni Nair).

0223-5234/$ – see front matter © 2013 Elsevier Masson SAS. All rights reserved.
http://dx.doi.org/10.1016/j.ejmech.2013.07.051

2. Results and discussion

2.1. Spectral and electrochemical analysis

The ESI-MS spectra of both the complexes are shown in Fig. S1 and S2. The mass spectrum of complex **1** exhibits base peak at *m*/*z* 424.00 which can be attributed to the complex cation $[Cu(Itpy)(NO_3)]^+$. The base peak at *m*/*z* 461.00 observed in the mass spectrum of complex **2** can be attributed to the complex cation $[Cu(Itpy)(ClO_4)]^+$. Coordinated water molecule is generally lost under the operating cone voltage [19]. The ESI-MS of complex **2** was analysed at low cone voltage (0.1 V). Under this condition the mass spectrum did exhibit a peak at *m*/*z* 201.53, which can be attributed to $[Cu(Itpy)(H_2O)_2]^{2+}$ species, which is obtained by loss of perchlorate from the coordination sphere. FTIR spectrum of **2** (Figs. S3, S4) shows strong band at 1383 cm^{-1} corresponding to the coordinated nitrate ion. Existence of single band clearly shows the bidentate nature of coordinated nitrate ion through two oxygen atom. Complex **2** shows broad band 1067–1158 cm^{-1} and a sharp band at 624 cm^{-1} corresponding to the asymmetric stretching and bending vibration mode of uncoordinated perchlorate ion. Both the complexes show broad band between 3086 and 3415 cm^{-1}, which can be attributed to the imidazole (–NH) nitrogen; broadness of the band indicate possible hydrogen bonding (probably to water molecule). Complexes **1** and **2** also show bands at 799 and 804 cm^{-1}respectively, which can be attributed to coordinated water molecule [20].

The electronic spectra of the complexes (Fig. S5) exhibit two ligand based transitions in the region 250–290 nm. Both the complexes shows intense MLCT band around 355 nm along with a shoulder peak around 338 nm. Both the complexes shows broad ligand field band in the region 700 nm. Absorption spectral data for the two complexes are shown in Table S1.

EPR spectrums of both the copper complexes have been recorded at 300 K as well as at 77 K. EPR spectrums of both the complexes are shown in Figs. S6, S7 and the corresponding spin Hamiltonian parameters are given in Table 1. From Table 1 it can be seen that the *g* values are in the order $g_{//} > g_{\perp} > g_e$ suggesting that the copper (II) complexes have approximate axial symmetry with d_{x2-y2} as ground state [21]. The ratio of $g_{//}/A_{//}$ is used to determine the degree of deviation from the perfect geometry. Complex **2** shows $g_{//}/A_{//}$ ratio 144 cm^{-1}, which is similar to the value, observed for $[Cu(Itpy)Cl]^{2+}$ complex, which exhibited moderate distortion from the plane of symmetry [22]. In the case of complex **1** $g_{//}/A_{//}$ value is 188 cm^{-1} indicating strong deviation from the square planar geometry. This is quite obvious from the crystal structure of the complex. Exchange interaction coupling constant G is another important parameter used to determine the nature of distortion. Usually complexes with $G > 4$ have negligible exchange interaction with parallel or slightly misaligned tetragonal axis, whereas complexes with $G < 4$ shows considerable exchange interaction of misaligned tetragonal axes. The G values computed for complexes **1** and **2** are 5.8 and 3.8 respectively. These values clearly show negligible exchange interaction with parallel tetragonal axes. The crystal packing (Fig. S8) observed for complex **1** also supports this fact. Orbital covalency parameter (α^2) was calculated using Eq. (1). Covalency parameter for complex **1** and **2** were 0.8136 and 0.7828

Table 1
EPR spin Hamiltonian parameter for complex **1** and **2**.

Complex	$g_{//}$	$g_{\perp}$	g_{iso}	$A_{//} \times 10^4(cm^{-1})$	$g_{//} A_{//}^{-1}(cm^{-1})$	*G*
(**1**)	2.3951	2.0677	2.0663	127	188	5.8
(**2**)	2.2763	2.0724	2.0552	158	144	3.8

Table 2
Electrochemical parameter for complex **1** and **2** in DMSO solvent using TBAP as supporting electrolyte.

Complexes	CV			DPV	ΔE_p [mV]	i_p/i_c
	E_{pa}	E_{pc}	$E_{1/2}$ [V]			
(**1**)	−0.156	−0.244	−0.200	−0.234	88	0.99
(**2**)	−0.162	−0.274	−0.218	−0.246	112	0.91

respectively. It is known that complexes with covalency parameter in the range of 0.5–1 show considerable covalent character [23]. The observed value of α^2 for the two complexes indicate that both the complexes have considerable covalent character.

$$\alpha^2 = \left(A_{///}/0.036\right) + \left(g_{//} - 2.0023\right) + (3/7)(g_{\perp} - 2.0023) + 0.04 \quad (1)$$

DMSO solution of both complexes **1** and **2** exhibit reversible electrochemical wave attributable to Cu(II)/Cu(I) redox process with $E_{1/2}$ −0.20 V and −0.22 V *vs* SCE. The higher Cu(II)/Cu(I) redox potential observed for complex **1** compared to that observed for complex **2** reflects the ligation of electron withdrawing nitrate with the metal centre in this complex. The electrochemical parameters obtained for the two complexes are given in Table 2.

2.2. X-ray crystallography

Complex **1** has also been characterized crystallographically. ORTEP diagram of complex **1** is shown in Fig. 1. It can be seen from the ORTEP diagram that Cu (II) ion has six coordinate geometry with the tridentate terpyridine ligand, a nitrate ion and a water molecule coordinated to the metal ion. The nitrate ion acts as a bidentate ligand. Three tertiary nitrogen from Itpy ligand and oxygen from the nitrate ion occupy the basal plane, while the axial sites are occupied by oxygen from the nitrate ion and oxygen from the coordinated water molecule. One of the oxygen of the coordinated nitrate ion is at longer distance from the central metal ion with Cu–O bond length of 2.79 A°, due to Jahn–Teller distortion. Overall, complex **1** has distorted octahedral geometry with perfect planar Itpy ligand.

π–π stacking interactions and H-bonding. The π–π stacking of **1** is an offset slipped stacking as shown in Fig. 2. However, aromatic Itpy is displaced in antiparallel manner due to hydrogen bonding

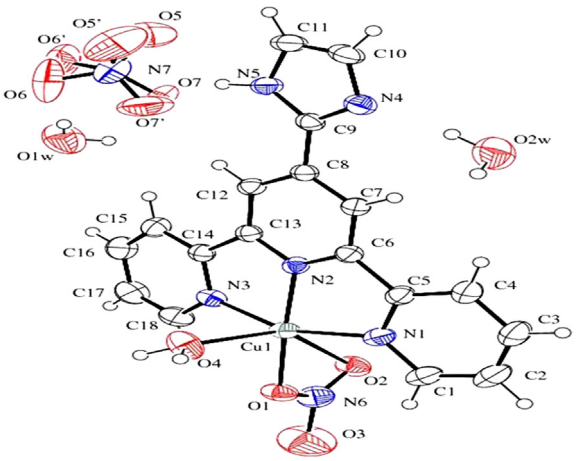

Fig. 1. ORTEP diagram of complex **1**.

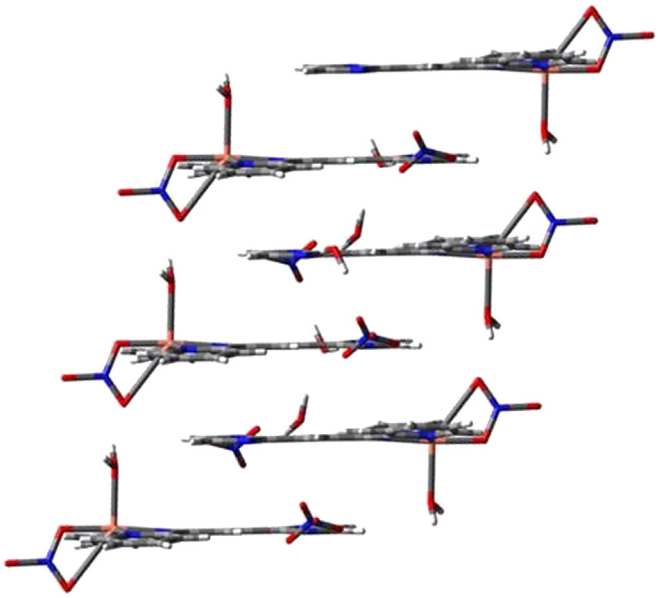

Fig. 2. Crystal packing diagram of complex **1** shows anti-parallel π–π stacking of Itpy ligand. H-bonding is omitted for clarity.

between the coordinated nitrate ion and water molecules with short distance of 3.390 A° between the Itpy units. Usual π–π stacking with offset slipped parallel arrangement is also present with longer distance of 7.180 A° between the Itpy units. Overall the π–π stacking of complex **1** looks like anti-parallel stacked Itpy with nitrate and water hydrogen bonded backbone.

Three different hydrogen bonds are present in the crystal structure of complex **1**. Two hydrogen bonds are present in imidazole head group nitrogen, one via uncoordinated nitrate ion and the other via crystalline water molecule. The third hydrogen bond is between oxygen of coordinated nitrate of one molecule and the hydrogen of coordinated water of another molecule. Hydrogen bond related bond lengths are shown in Table 3. Multiple hydrogen bonding networks brings the planar Itpy ligands closer. This results in rigid anti-parallel π–π stacking arrangement (Fig. 2). It is pertinent to mention here that another complex of Cu(II) with terpy as the tridentate ligand and nitrate as a monodentate ligand, $[Cu(tpy)(NO_3)_2(H_2O)]$ has been reported previously [18]. Behaviour of nitrate ion in this complex is different from its behaviour in complex **1**, where nitrate ion behaves as bidentate ligand. The stacking distance in this complex is longer than the one observed in complex **1** due to the presence of nitrate groups in both axial positions and due to the absence of imidazole head group in this complex.

Table 3
Hydrogen bonds for **1** [A and deg.].

D-H…A	d(D-H)	d(H…A)	d(D…A)	<(DHA)
O(4)-H(4A)…O(1W)[a]	0.920(10)	1.868(13)	2.772(4)	167(3)
O(4)-H(4B)…O(2)[b]	0.914(10)	1.872(16)	2.743(3)	159(3)
N(5)-H(5)…O(7)	0.963(10)	2.02(2)	2.934(14)	157(3)
N(5)-H(5)…O(5)	0.963(10)	2.17(3)	2.992(10)	143(3)
O(2W)–H(2B)…N(4)	0.925(10)	1.938(13)	2.857(4)	171(4)
O(2W)–H(2A)…O(6)[c]	0.929(9)	2.002(9)	2.922(13)	170(5)
O(1W)–H(1B)…O(6)	0.929(10)	2.04(2)	2.955(16)	167(4)
O(1W)–H(1A)…O(2W)[d]	0.933(10)	1.975(13)	2.897(5)	169(4)

Symmetry transformations used to generate equivalent atoms.
[a] $x-1/2, -y+1/2, z-1/2$.
[b] $x-1,y,z$.
[c] $-x+1, -y, -z+1$.
[d] $-x+2, -y, -z+1$.

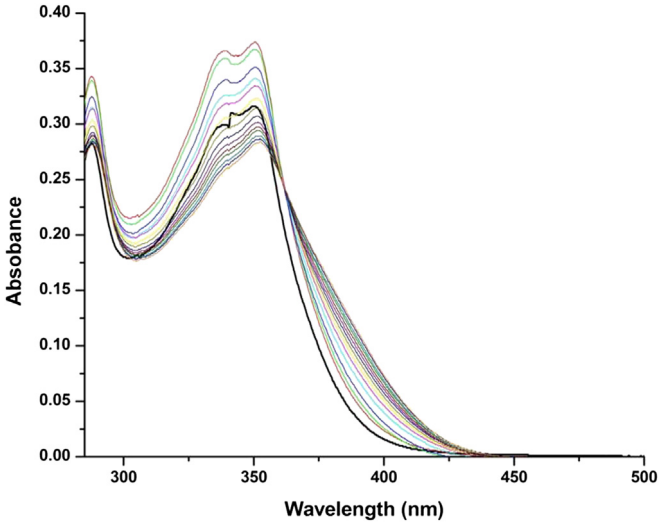

Fig. 3. Absorption spectral titration of complex **1** in the presence of increasing amount of CT DNA.

2.3. DNA binding studies

2.3.1. Absorption titration

The changes in the CT band (354 nm) of both the complexes were monitored in the presence of increasing concentration of CT DNA (Figs. 3 and 4). A clear isosbestic point appeared at 362 nm for complex **1** and at 361 nm for complex **2**, suggesting that only two species, free complex and DNA bound complex, are present in equilibrium during titration. Interestingly, both the complexes showed hyperchromism till the DNA to complex ratio reached one ($r = 1$). Subsequent increase in the concentration of the DNA led to decrease in the intensity of the CT bond and it reached a saturation point at $r = 14$ for complex **1** and 16 for complex **2**. This decrease in intensity of the CT band was accompanied by considerable red shift in the spectral band. These observations clearly show that both these complexes show dual mode of DNA binding. It is possible that initially because of the stacking within the metal complexes (as has been observed in the crystal structure of complex **1**) the complexes bind DNA electrostatically and at higher concentration of DNA the

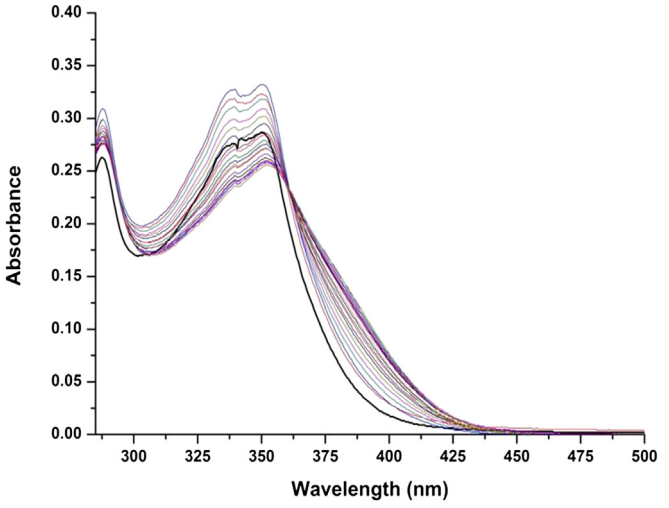

Fig. 4. Absorption spectral titration of complex **2** in the presence of increasing amount of CT DNA.

complexes get destacked and get intercalated between DNA bases. Such dual mode of DNA binding by a Ru (II) complex has previously been reported [24]. The DNA binding constant obtained through non-linear regression analysis of the spectral data are $K_{b1} = (4.23 \pm 0.12) \times 10^4\ M^{-1}$ and $K_{b2} = (5.92 \pm 0.18) \times 10^3\ M^{-1}$ for complex **1** and $K_{b1} = (2.01 \pm 0.08) \times 10^4\ M^{-1}$ and $K_{b2} = (3.21 \pm 0.12) \times 10^4\ M^{-1}$ for complex **2**. In the present case the K_{b2} of complex **2** is much larger than K_{b2} of complex **1**. This may be due to the presence of perchlorate, which is a weak ligand, in complex **2**. The perchlorate in this case can be easily replaced by water in aqueous solution. Whereas, in the case of complex **1**, coordinated nitrate is retained even in aqueous solution. Because of the presence of the nitrate, which promotes stacking of the complexes due to its hydrogen bonding with coordinated water, in this case destacking in the presence of DNA is probably less efficient and this leads to lower K_{b2} value.

2.3.2. Circular dichroism

The conformation and helicity changes of CT DNA in the presence of the two copper (II) complexes were studied using circular dichroism and the results are shown in Fig. 5 and S9. The CD spectrum of B-DNA shows a positive peak at 275 nm due to base stacking and a negative peak at 245 nm due to helicity [25]. DNA was incubated for 30 min with different concentrations of the two copper (II) complexes (r ([DNA]/[Complex] = 5 to 1.25). Intensity of both the positive and negative band of DNA has been found to decrease in the presence of the two complexes. However, the change in the intensity of the negative peak is more pronounced than the change in the positive peak intensity. This observation clearly shows that both complexes **1** and **2** affect the helicity of B-DNA.

2.3.3. DNA cleavage study

Chemical nuclease activity of the complexes was studied in the absence and the presence of oxidizing agent H_2O_2 (Fig. 6a, b). Without any external agent complex **1** was able to bring about conversion of SC form of DNA to NC form. However, the concentration of the complex needed to bring about this conversion was 40 μM or more and the complex and DNA had to be incubated for at least 24 h (data's not shown). On the other hand, complex **2** did not bring about any DNA cleavage in the absence of added coreagent

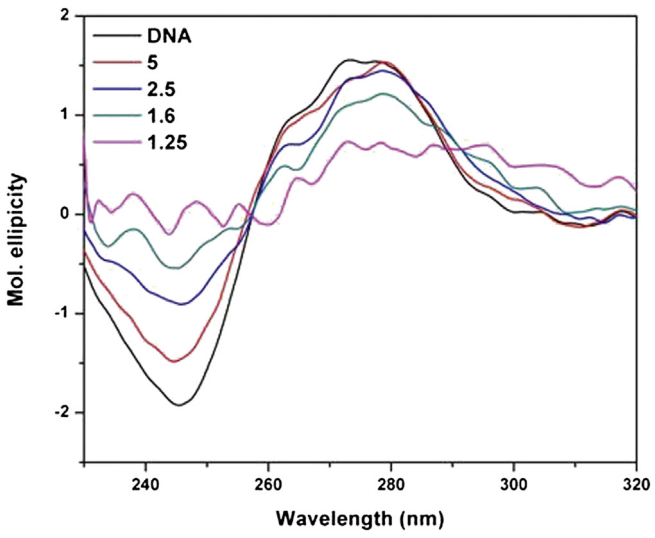

Fig. 5. Circular dichroic spectra of CT DNA in the presence of increasing amount of complex **1**.

even at high metal complex concentration and longer incubation time. This shows that complex **1** has marginal ability of inducing hydrolytic cleavage of DNA, whereas complex **2** does not possess any such activity. Both the complexes were able to convert SC DNA to NC form, even at low concentration, within 10 min incubation time, in the presence of H_2O_2 (Fig. 6a, b). At a metal complex concentration of 80 μM, both the copper (II) complexes were able to convert NC form of DNA to the linear form in the presence of H_2O_2. DNA cleavage experiments performed in the presence of DMSO did not lead to any DNA cleavage (data not shown). This clearly indicates that the observed DNA cleavage by the two copper (II) complexes in the presence of H_2O_2 is due to hydroxyl radicals.

2.4. Cytotoxicity

2.4.1. MTT assay

Cytotoxicity of the two complexes towards A549 human lung cancer cell line was studied by 3-(4, 5-dimethylthiazol-2-yl)-2, 5-diphenyltetrazolium bromide (MTT) assay. Cell viability was analysed by monitoring the characteristic peak of formazan at 595 nm. From the percentage growth a dose response curve was generated and GI_{50} values were interpolated from the growth curves shown in Fig. S10. The GI_{50} values for complex **1** and complex **2** were found to be 0.81 μM and 0.64 μM respectively. It is pertinent to note that the reported cytotoxicity of $[Cu(tpy)(NO_3)_2(H_2O)]$ which too has a tridentate terpy ligand and nitrate ion coordinated to the central metal ion is less than that of complex **1** [18]. This difference in the observed cytotoxicity between **[**$Cu(tpy)(NO_3)_2(H_2O)$] and complex **1** may be attributed to the fact that, complex **1** due to the presence of planar imidazole head group, intercalates easily between the base pairs of DNA and the hydrogen bonding between the N and NH present in the ligand and the DNA bases stabilizes the binding of the complex to DNA.

2.4.2. Nuclear stains (PI and AO/EB dual staining)

Fluorescent staining helps identify cells of interest. Using different fluorescent dyes, one can study the apoptotic populations after the drug treatment. Fluorescent stains generally used for identifying live and dead cells are acridine orange (AO), ethidium bromide (EB) and propidium iodide (PI). In this study, A549 lung cancer cell lines with different concentration of complexes were stained using PI stain and AO/EB dual stains. PI and EB are non-permeable to the live cells, whereas AO is permeable to both live and dead cells [26]. Dose dependent apoptosis inducing ability of complex **1** and **2** studied using these three fluorescent stains are shown in Fig. S7,11 respectively. Control images are shown in Fig. S12. From Fig. S11 one can see that as the concentration of complex **1** increase from 3.9 μM to 15.6 μM the intensity of green fluorescence due to AO stain decreases, indicating that population of live cells decrease with increase in the concentration of complex **1**. In the presence of 15.6 μM complex **1** bright green patches are seen which is an indication of early apoptosis [27]. It is also evident from the Fig. S11 that as the complex concentration increases, the orange fluorescence due to EB stain increases, indicating an increase in the population of dead cells. The merged figures clearly show that as the complex concentration increases the green fluorescence decreases and the orange fluorescence increases, indicating cell death at higher concentration of the complex. The early apoptosis brought about by the complex at 15.6 μM of complex **1** too is evident from the merged image as bright green patches. From the fluorescence microscopic images of PI stained cells shown in Fig. S11 one can clearly see nuclear fragmentation, particularly at 15.6 μM of complex **1**. Fluorescence microscopy images of cells treated with complex **2** shown in Fig. 7 clearly indicate that in this case even 3.9 μM of the complex is able to bring about early

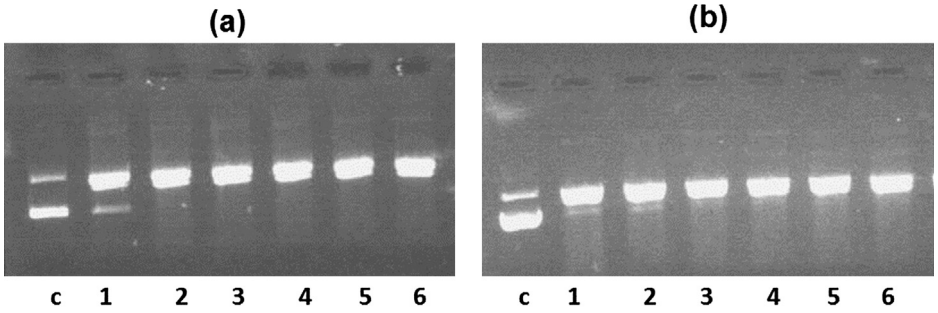

Fig. 6. Agarose gel electrophoretic analysis of complex **1** and **2**. **a**) Complex **1**, lane c (control), lane 1–6, 20, 40, 60,80, 100 and 120 μM (**1**)+20 μM H_2O_2. **b**) Complex **2**, lane c (control), lane 1–6, 20, 40, 60,80, 100 and 120 μM (**2**) + 20 μM H_2O_2.

apoptosis, as evident from the bright green patches in the AO stained image. Results of PI staining of complex **2** treated cells show initial nuclear condensation, blebbing and apoptotic body formation at 15.6 μM of the complex, which is typical of late apoptosis or necrosis. Staining results of % of apoptotic cells by complexes are shown in Table. S2.

2.4.3. Fluorescence-activated cell sorting (FACS) analysis of cell cycle arrest

FACS analysis of the control A549 cells show that 75.5% of the cells are in G_0/G_1 phase, which is the growth phase before replication; 19.2% of the cells are in the S phase, which is the DNA synthesis phase where DNA replication occurs and 5.1% are in the G_2/M phase where cell division occurs. Copper (II) complex concentration depended cell cycle arrest is shown in Fig. 8. It can be clearly seen from the Figure that in the presence of 0.5 μM of complexes **1** and **2** the S phase of cell cycle shows marginal reduction. It is pertinent to note that in the presence of 0.5 μM of the two copper (II) complexes, no sub G_0/G_1 phase, which is a marker for induction of apoptosis, is observed in the cell cycle. This indicates that 0.5 μM of the two complexes do not bring about apoptosis of A549 cells. In the presence of 2.5 μM of complexes **1** and **2** however, the S phase decreases to 17.1% and 13.2% respectively and the G_2/M phase decreases to 1.4% and 1.9% respectively. More importantly, at this concentration of the two complexes cell cycle analysis also shows 3.3% and 8.1% of sub G_0/G_1 phase. Appearance of G_0/G_1 phase in the cell cycle clearly indicates that 2.5 μM of the two complexes bring about apoptosis of A549 cells. These results (Table S3) also indicate that complex **2** is more effective than complex **1** in bringing about apoptosis of A549 cells.

3. Conclusion

Two copper (II) complexes, **1** and **2** have been synthesized and characterized through various spectroscopic techniques. Complex **1** has also been characterized crystallographically. Because of the presence of multiple hydrogen bonding, the molecules are stacked in an anti-parallel fashion in their crystalline state. Both these complexes exhibit dual mode of binding to DNA with $K_{b1} = (4.23 \pm 0.12) \times 10^4$ and $Kb_2 = (5.928 \pm 0.18) \times 10^3$

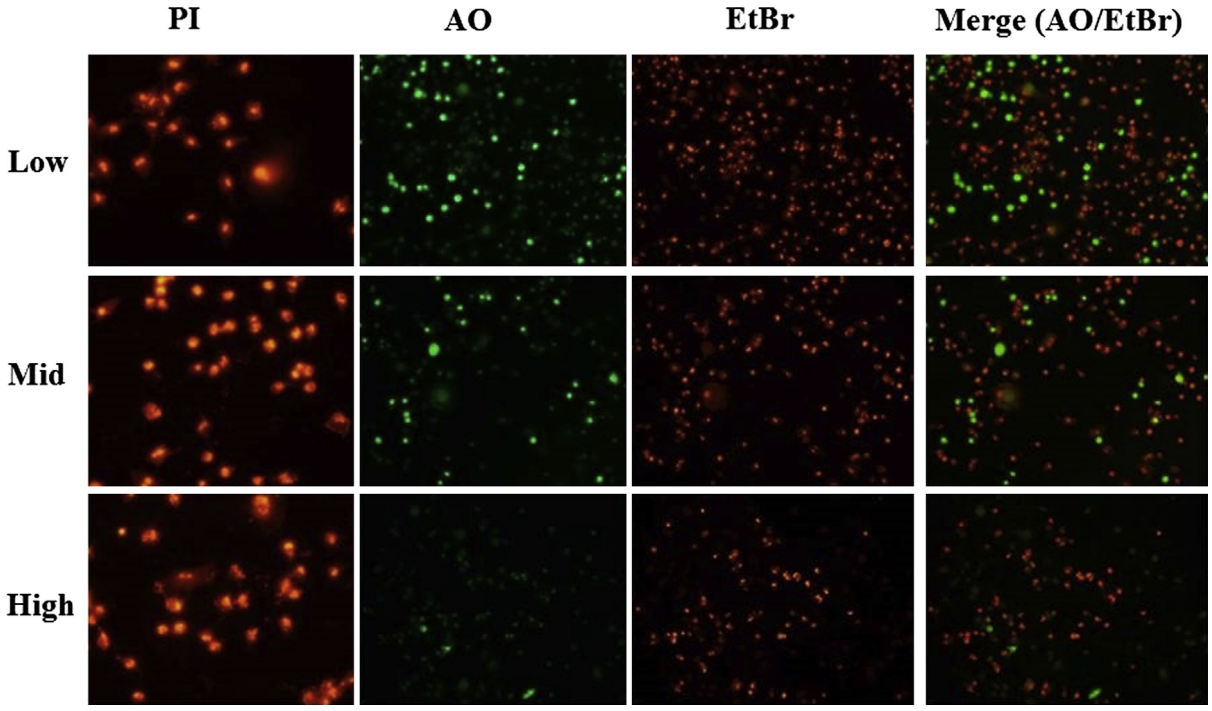

Fig. 7. Fluorescent micrograph of Propidium iodide (PI) and acridine orange/ethidium bromide (AO/EtBr) nuclear stained A549 cells lines treated with different concentration of complex **2**, Low (3.9 μM), Mid (7 μM), High (15.6 μM).

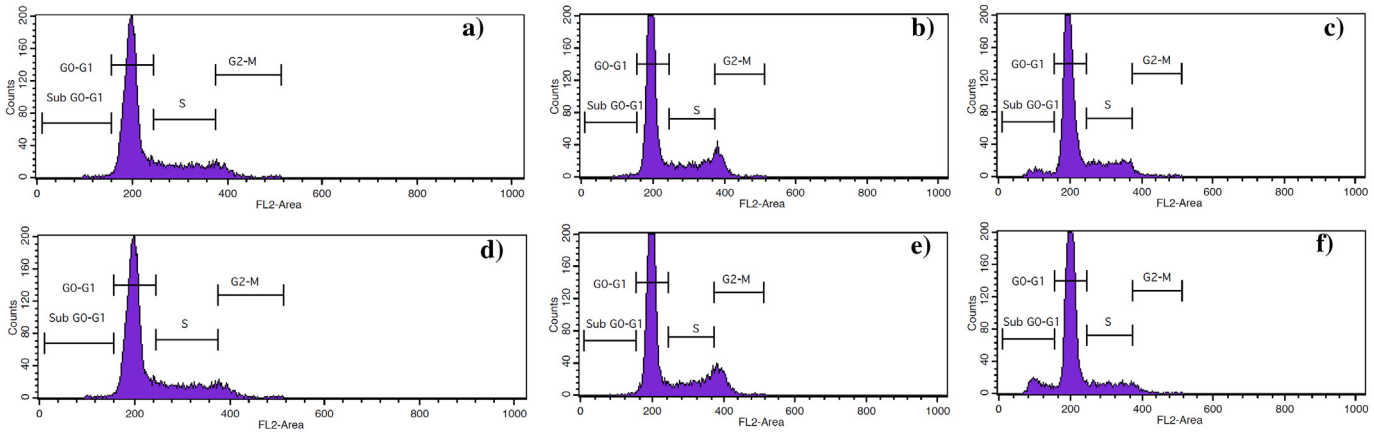

Fig. 8. FACS analysis of DNA from control and complex treated A549 cells. (a) control for **1**, (b) 0.5 μM **1**, (c) 2.5 μM **1**; (d) control for **2**, (e) 0.5 μM **2**, (f) 2.5 μM **2**.

for complex **1** and $K_{b1} = (2.0182 \pm 0.08) \times 10^4$ and $K_{b2} = (3.214 \pm 0.12) \times 10^4$ for complex **2**. At lower concentration of DNA the stacked complexes bind to DNA non-intercalatively. However, higher concentration of DNA promotes destacking of the complexes, resulting in their intercalative binding to DNA. Both the complex **1** and **2** has been found to bring about DNA cleavage in the presence of H_2O_2. Both these complexes were found to be cytotoxic towards lung carcinoma cell line with GI_{50} values 0.81 μM and 0.64 μM for complexes **1** and **2** respectively. The ability of these two complexes to induce apoptosis to the cancerous cells has been confirmed through fluorescence microscopic images of PI stained cells and FACS analysis. Complex **2** has been found to be more effective in inducing apoptosis to the cells than complex **1** and this is reflected in their GI_{50} values too. Complex **2** is more strongly intercalated to DNA than complex **1,** as reflected in their K_{b2} values and this relatively stronger intercalation of complex **2** is probably responsible for its higher cytotoxicity.

4. Experimental methods

4.1. Materials and methods

The materials used in this investigation such as 2-acetyl pyridine, imidazole-2-carboxaldehyde, copper (II) perchlorate hexahydrate and copper (II) nitrate hexahydrate were purchased from Aldrich Chemicals and used as received. Other materials like sodium hydroxide, ammonium acetate, sodium chloride and solvents like methanol, dimethyl sulfoxide and acetonitrile were of reagent grade. Calf thymus (CT DNA) and supercoiled pUC19 (Cesium chloride purified) DNA were purchased from Bangalore Genie (India). Agarose (molecular biology grade) and ethidium bromide (EB) were from Sigma. DNA binding studies were performed in 50 mM NaCl/5 mM Tris, pH 7.2 buffer. The ligand, imidazole–terpyridine was prepared using published procedures [28]. Human lung adenocarcinoma cells, A549 was purchased from National Centre for Cell Science, Pune, India. A549 cell line was grown in DMEM (Dulbecco's Modified Eagle's Medium), containing 2 mM glutamine, 0.55 mM L-arginine, 0.24 mM L-asparagine monohydrate supplemented with 10% heat inactivated Fetal Calf Serum (FCS) and antibiotics penicillin/streptomycin/gentamicin.

4.2. Physical measurements

Electronic spectra were recorded using a Perkin–Elmer Lambda 35 double beam spectrophotometer. The elemental analysis was performed using an EURO EA 3000–Single CHN analyser. Electrospray ionization mass spectra (ESI-MS) were obtained from Thermo Finnigan LCQ 6000 advantage max ion trap mass spectrometer using acetonitrile as carrier solvent. Voltammetry experiments were carried out by using a standard three-electrode system comprising of glassy carbon working electrode of 3 mm diameter, platinum auxiliary electrode and saturated calomel reference electrode (SCE). Glassy carbon electrode surface was polished with alumina, and then cleaned ultrasonically. The samples were prepared in DMSO, and the solutions were deoxygenated by purging nitrogen gas for 10 min prior to the measurements. The experiments were carried out with a metal complex to supporting electrolyte concentration ratio 1:100. Tetrabutylammonium perchlorate (TBAP) was used as a supporting electrolyte. EPR spectral analysis was performed using Bruker EMX computer controlled spectrometer operating at X-band frequencies (~9.5 GHz). Microwave generation was by means of Gunn diode, (Bruker ER041 XG Microwave Bridge X band). Flow cytometric analysis was performed using BD FACS calibre instrument. Fluorescence of cells was measured using inverted fluorescent microscope from Nikon, Japan.

4.3. Synthesis of complexes

4.3.1. [Cu (Itpy) (NO_3) (H_2O)] (NO_3). 2H_2O (**1**)

A warm methanol solution (5 ml) of Itpy (300 mg, 1 mM) was added to a solution of $Cu(NO_3)_2 \cdot 3H_2O$ (242 mg, 1 mM) in methanol (10 ml) and then stirred at room temperature for 3 h. The resulting clear solution was heated to boil and kept aside for crystallization. The crystals obtained were recrystallized from methanol-water (10:1). Yield 89%. Crystals suitable for X-ray diffraction were obtained by ether diffusion method. Elemental analysis data for (**1**) $C_{18}H_{19}CuN_7O_9$; Calculated (%) C 39.97, H 3.54, N 18.13; found (%) C 38.86, H 3.62, N 17.98. The complex was soluble in acetonitrile, ethanol and DMSO and partially soluble in water.

4.3.2. [Cu (Itpy) (ClO_4) (H_2O)] (ClO_4) (**2**)

Hot methanolic solution (5 ml) of Itpy (300 mg, 1 mM) was added to methanolic solution of $Cu(ClO_4)_2.6H_2O$ (371 mg, 1 mM) and then the solution was stirred at room temperature for 3 h. The resulting solution was filtered and kept aside for recrystallization. Yield 86%. Elemental analysis data for (**2**) $C_{18}H_{15}Cl_2CuN_5O_9$; Calculated (%) C 37.29, H 2.61, N 12.08; found (%) C 37.18, H 2.57, N 11.96. The complex was soluble in acetonitrile, ethanol and DMSO and partially soluble in water.

Caution: *Perchlorate salts of metal complexes are potentially explosive and should be handled in small quantities with care.*

4.4. X-ray crystallographic data collection and refinement of the structures

Crystals of complex **1** was cut into suitable size and mounted on Kappa Apex 2 CCD diffractometer equipped with graphite monochromated Mo Kα radiation ($\lambda = 0.71073$ Å). The intensity data were collected using ω and φ scans with frame width of 0.5°. The frame integration and data reduction were performed using Bruker SAINT-Plus (version 7.06a) software. The multi-scan absorption corrections were applied to the data using SADABS (Bruker 1999) program. The structure was solved using SIR92 [29]. Full-matrix least squares refinement was performed using SHELXL-97 programs [30]. All the non-hydrogen atoms were refined with anisotropic displacement parameters. All the hydrogen atoms could be located in a difference Fourier map. However, they were relocated at chemically meaningful positions and were given riding model refinement. The refinement of water hydrogen atoms were restrained such that they remain in the vicinity of the respective difference peak. Crystallographic parameters are shown in Table 4. Important bond lengths and bond angles are given in (Table 5).

4.5. DNA binding study

4.5.1. Absorption spectral studies

Absorption titrations were performed by fixing the complex concentration (20 μM) constant and varying the CT DNA concentration (0–380 μM). To nullify the absorbance changes due to DNA, an equal volume of DNA was added to both the reference cell and the sample cells. Titration was carried out till the absorbance changes were almost negligible. From the absorption titration studies, the nature of equilibrium DNA binding constants, K_b, was determined using Eq. (2) which includes binding site size by regression analysis [31–33].

$$\frac{(\varepsilon_a-\varepsilon_f)}{(\varepsilon_b-\varepsilon_f)} = \frac{\left[b-\left(\frac{b^2-2K_b^2C_t[DNA]}{s}\right)\right]^{1/2}}{2K_bC_t} \qquad (2)$$

$$b = \frac{1+K_bC_t+K_b[DNA]}{2s}$$

Where ε_a is the extinction coefficient for the MLCT absorption band at a given DNA concentration. ε_f is the extinction coefficient of the free complex in solution, ε_b is the extinction coefficient of the complex when fully bound to DNA, K_b is the equilibrium constant, C_t is the total metal complex concentration, [DNA] is DNA concentration in base pairs and s is the binding site size in base pairs.

Table 4
Crystal data and structure refinement for complex 1.

Empirical formula	C18H19 Cu N7 O9
Formula weight	540.94
Temperature	293(2) K
Wavelength	0.71073 A
Crystal system, space group	Monoclinic, P21/n
Unit cell dimensions	a = 7.1805(2) A alpha = 90 deg. b = 22.8433(6) A beta = 100.7790(10) deg. c = 14.1967(3) A gamma = 90 deg.
Volume	2287.55(10) A^3
Z, Calculated density	4, 1.571 Mg/m^3
Absorption coefficient	1.019 mm^-1
F(000)	1108
Crystal size	0.30 × 0.25 × 0.20 mm
Theta range for data collection	2.30–32.07 deg.
Limiting indices	$-10 \le h \le 10$, $-34 \le k \le 33$, $-21 \le l \le 21$
Reflections collected/unique	33885/7968 [R(int) = 0.0573]
Completeness to theta = 32.07	99.8%
Absorption correction	Semi-empirical from equivalents
Max. and min. transmission	0.8221 and 0.7497
Refinement method	Full-matrix least-squares on F^2
Data/restraints/parameters	7968/14/373
Goodness-of-fit on F^2	1.020
Final R indices [I > 2sigma(I)]	$R1$ = 0.0501, wR2 = 0.1230
Indices (all data)	$R1$ = 0.1083, wR2 = 0.1483
Largest diff. peak and hole	0.478 and −0.530 e.A^−3

Table 5
Important bond lengths [A] and angles [deg] for complex **1**.

Important band lengths	
O(1)-Cu(1)	1.9063(18)
O(4)-Cu(1)	2.264(2)
N(1)-Cu(1)	2.043(2)
N(2)-Cu(1)	1.9296(19)
N(3)-Cu(1)	2.049(2)
Important band angles	
N(6)-O(1)-Cu(1)	113.56(16)
O(1)-Cu(1)-N(2)	175.70(7)
O(1)-Cu(1)-N(1)	99.58(9)
N(2)-Cu(1)-N(1)	79.73(8)
O(1)-Cu(1)-N(3)	100.32(9)
N(2)-Cu(1)-N(3)	79.54(8)
N(1)-Cu(1)-N(3)	156.81(8)
O(1)-Cu(1)-O(4)	90.81(8)
N(2)-Cu(1)-O(4)	93.47(8)
N(1)-Cu(1)-O(4)	103.86(8)
N(3)-Cu(1)-O(4)	87.65(9)

4.5.2. Circular dichroism

CD spectra of CT DNA (200 μM) were analysed in the absence and presence of increasing concentration of complexes. Spectra were run for R values 5, 2.5, 1.6 and 1.25 (R = [DNA]/[complex]). CD spectra were taken as the average of three independent scans between 220 and 330 nm using JASCO J-815 CD spectrometer with 150 W Xe arc lamp.

4.6. Antiproliferative activity

4.6.1. Cell culture

The A549 cells were grown in a RPMI 1640 medium supplemented with 10% fetal bovine serum and antibiotics. For the MTT assay, the cells were grown in 25 cm × 25 cm × 25 cm tissue culture flasks containing RPMI 1640 medium as culture medium supplemented with 10% FCS, 100 U/ml penicillin, 100 μg/ml streptomycin (GIBCO) and grown at 37 °C under a humidified atmosphere of 95% air and 5% CO_2. Cells were allowed to adhere for 4 h. When a cell density in a culture flask reached 70–80% confluence, they were trypsinized and seeded in 96-well plates. Each well had a cell density of 3×10^4 cells and they were grown for 24 h.

4.6.2. MTT assay

Cytotoxicity (MTT) assay was performed following the method described by Carmichael et al. [34], and percentage of cell viability was determined by spectrophotometric determination of accumulated formazan derivative in treated cells at 570 nm in comparison with the untreated ones. Test complexes were added as 2× concentration to the cell in 100 μl volume and the concentration range were: 100, 10, 1, 0.1 and 0.01 μM. The plates were further incubated for 48 h in the CO_2 incubator. MTT solution was composed of 3-(4,5-dimethylthiazol-2-yl)-2,5-diphenyl tetrazolium bromide (MTT) at 5 mg/ml in phosphate buffered saline (1.5 mM KH_2PO_4, 6.5 mM Na_2HPO_4, 137 mM NaCl, 2.7 mM KCl; pH 7.4). From this solution 50 μl was pipette out into each well to achieve 1 mg/ml as final concentration. The plate was further incubated for 2.30 h in an incubator and the medium was carefully decanted. The formazan crystals were air dried in a dark place and dissolved in 100 μl DMSO and the plates were mildly shaked at

room temperature and the absorbance at 570 nm was measured using Synergy H4 micro plate reader. From the absorbance values the percentage cell growth were calculated using the following formula:

$$\text{Percentage growth} = 100 \times (T - T_0)/(C - T_0)$$

Where T is absorbance of copper (II) complex treated cells; C is the absorbance of control cells; T_0 is the absorbance at time zero.

4.6.3. Cellular morphology assessment through acridine orange/ethidium bromide (AO/EB) staining (dual staining)

Ethidium bromide/acridine orange staining was carried out by the method of Gohel et al. [35] A549 cells were plated at a density of 5×10^4 in 6-well plates. They were allowed to grow at 37 °C in a humidified CO_2 incubator until they were 70–80% confluent. Then cells were treated with different concentrations of complexes **1** and **2** for 24 h. The culture medium was aspirated from each well and cells were gently rinsed twice with PBS at room temperature. Then equal volumes of cells from control and drug treated were mixed with 100 μl of 1:1 ethidium bromide and acridine orange and viewed immediately by fluorescence microscopy. The percentage of apoptotic cells was determined [% of apoptotic cells = (total number of apoptotic cells/total number of cells counted) × 100].

4.6.4. Propidium iodide staining (PI)

Propidium iodide staining was carried out by the method of Chandramohan et al. [36] A549 cells were plated at a density of 5×10^4 in 6-well plates. They were allowed to grow at 37 °C in a humidified CO_2 incubator until they were 70–80% confluent. Then cells were treated with different concentrations of complexes **1** and **2** for 24 h. Culture medium was aspirated from each well and cells were gently rinsed twice with PBS at room temperature, before fixing in methanol: acetic acid (3:1 v/v) for 10 min, and stained with 50 μg/ml propidium iodide for 20 min. Nuclear morphology of apoptotic cells was examined by fluorescence microscopy and at least 1×10^3 cells were counted for assessing apoptotic cell death.

4.6.5. Analysis of DNA content by FACS

When cell density in a culture flask reached 70–80% confluence, they were trypsinized and seeded in 6-well plates at a density of $5–8 \times 10^5$ cells/well and grown for 24 h. 0.5 μM and 2.5 μM of complexes **1**, and **2** were added to the cells and grown for 24 h. Control cultures were treated with DMSO. After the respective experimental period, the cells were trypsinized and collected in a falcon tube and washed with phosphate buffered saline (PBS). After washing the cells with PBS, the cells were fixed by gently adding ice-cold 70% ethanol (drop by drop) with simultaneous vortexing and left overnight at 4 °C. On the day of analysis, samples were centrifuged for 10 min at 1500 RPM. The supernatant was discarded, and the pellets were resuspended in PBS. This step was repeated again to remove ethanol. Following this, the cells were then resuspended in PBS containing 0.5% Triton X-100, 0.1 mg/ml RNase and 40 μg/ml propidium iodide in a dark room. Triton-X and RNAase were added to permeabilize the cell membrane and eliminate RNA. After 30 min incubation at 37 °C, the cells were analysed on a flow cytometer, equipped with an air-cooled argon laser providing 15 mW at 488 nm with standard filter setup. 10,000 events were collected and the percentages of each cell cycle phases were analysed using Cell quest Pro software (Becton Dickinson, USA).

Propidium iodide (PI) is the most widely used fluorescent dye for staining DNA in whole cells (or isolated nuclei). PI intercalates into the DNA helix of fixed and permeabilized cells. Because PI can stain both double-stranded RNA and DNA, cells must be treated with RNase to ensure that PI staining is DNA specific. PI does not cross the plasma membrane of viable cells. However, it can readily enter dead cells that have damaged plasma membranes, and can stain their cellular DNA.

Acknowledgements

V.M.M. acknowledges CSIR-India for a fellowship and IITM-SAIF for crystal structure analysis.

Appendix A. Supplementary data

Supplementary data related to this article can be found at http://dx.doi.org/10.1016/j.ejmech.2013.07.051.

References

[1] A.V. Klein, T.W. Hambley, Chem. Rev. 109 (2009) 4911–4920.
[2] B. Rosenberg, L. VanCamp, J.E. Trosko, V.H. Mansour, Nature 222 (1969) 385–386.
[3] D.D. Von Hoff, M. Rozencweig, Adv. Pharmacol. Chemother. 16 (1979) 273–298.
[4] a) D. Chen, V. Milacic, M. Frezza, Q.P. Dou, Curr. Pharm. Des. 15 (2009) 777–791; b) G. Murtaza, M.K. Rauf, A. Badshah, M. Ebihara, M. Said, M. Gielen, D. de Vos, E. Dilshad, B. Mirza, Eur. J. Med. Chem. 48 (2012) 26–35.
[5] a) M. Frezza, S. Hindo, D. Chen, A. Davenport, S. Schmitt, D. Tomco, Q.P. Dou, Curr. Pharm. Des. 16 (2010) 1813–1825; b) T.K. Goswami, S. Gadadhar, B. Gole, A.A. Karande, A.R. Chakravarty, Eur. J. Med. Chem. 63 (2013) 800–810.
[6] a) I. Ott, R. Gust, Archiv. Der. Pharmazie. 340 (2007) 117–126; b) D. Senthilraja, N.S.P. Bhuvanesh, K. Natarajan, Eur. J. Med. Chem. 46 (2011) 4584–4594.
[7] B.M. Zeglis, V.C. Pierre, J.K. Barton, Chem. Commun. 44 (2007) 4565–4579.
[8] R.A. Festa, D.J. Thiele, Curr. Biol. 21 (2011) 877–883.
[9] J.D. Watson, F.H. Crick, Nature 171 (1953) 737–738.
[10] J.D. Watson, F.H. Crick, Nature 171 (1953) 964–967.
[11] S.S. Bhat, A.A. Kumbhar, H. Heptullah, A.A. Khan, V.V. Gobre, S.P. Gejji, V.G. Puranik, Inorg. Chem. 50 (2011) 545–558.
[12] P. Jaividhya, R. Dhivya, M.A. Akbarsha, M. Palaniandavar, J. Inorg. Biochem. 114 (2012) 94–105.
[13] F.V. Pamatong, C.A. Detmer, J.R. Bocarsly, J. Am. Chem. Soc. 118 (1996) 5339–5345.
[14] O. Kovaleva, V. Tsvetkov, A. Shchyolkina, O. Borisova, V.O. shevskaya, A. Makarenkov, A. Semeikin, A. Shtil, D. Kaluzhny, Eur. Biophys. J. 41 (2012) 723–732.
[15] V.M. Manikandamathavan, R.P. Parameswari, T. Weyhermuller, H.R. Vasanthi, B.U. Nair, Eur. J. Med. Chem. 46 (2011) 4537–4547.
[16] K.M. Guckian, B.A. Schweitzer, R.X. Ren, C.J. Sheils, D.C. Tahmassebi, E.T. Kool, J. Am. Chem. Soc. 122 (2000) 2213–2222.
[17] K.M. Guckian, T.R. Krugh, E.T. Kool, J. Am. Chem. Soc. 122 (2000) 6841–6847.
[18] a) D.D. Li, J.L. Tian, W. Gu, X. Liu, H.H. Zeng, S.P. Yan, J. Inorg. Biochem. 105 (2011) 894–901; b) V.M. Manikandamathavan, V. Rajapandian, A.J. Freddy, T. Weyhermuller, V. Subramanian, B.U. Nair, Eur. J. Med. Chem. 57 (2012) 449–458.
[19] V.M. Manikandamathavan, M. Kavitha, V. Uma, R.P. Parameswari, Hannah R. Vasanthi, B.U. Nair, Polyhedron 30 (2011) 1604–1611.
[20] a) K.Nakamota, Infrared and Raman Spectra of Inorganic and Coordination Compounds. third ed. John Wiley and Sons, New York, 228; b) N. Raman, S. Ravichandran, C. Thangaraja, J. Chem. Sci. 116 (2004) 215–219.
[21] A.W. Addison, Copper coordination chemistry, in: K.D. Karlin, J. Zubieta (Eds.), Biochemical and Inorganic Perspectives, Adenine, Guilderland, New York, 1983, p. 109.
[22] J. Peisach, W.E. Blumberg, Arch. Biochem. Biophys. 165 (1974) 691–708.
[23] V. Uma, M. Kanthimathi, J. Subramanian, B.U. Nair, Biochim. Biophys. Acta 1760 (2006) 814–819.
[24] G. Sathyaraj, T. Weyhermuller, B.U. Nair, Eur. J. Med. Chem. 45 (2010) 284–291.
[25] V.I. Ivanov, L.E. Minchenkova, A.K. Schyolkina, A.I. Poletayev, Biopolymers 12 (1973) 89–110.
[26] J. Steigerova, J. Oklestkova, M. Levkova, L. Rarova, Z. Kolar, M. Strnad, Chem. Biol. Interact. 188 (2010) 487–496.
[27] R. Loganathan, S. Ramakrishnan, E. Suresh, A. Riyasdeen, M.A. Akbarsha, M. Palaniandavar, Inorg. Chem. 51 (2012) 5512–5532.
[28] G.W.V. Cave, C.L. Raston, J. Chem. Soc. Perkin Trans. 1 (2001) 3258–3264.
[29] A. Altomare, G. Cascarano, C. Giacovazzo, A. Guagliardi, J. Appl. Crystallogr. 26 (1993) 343–350.
[30] G. M. S. ShelXL97, University of Gottingen, Germany, 1997. ShelXtl V. 5, Siemens Analytical X-Ray Instruments, Inc., 1994.

[31] S.R. Smith, G.A. Neyhart, W.A. Karlsbeck, H.H. Thorp, New J. Chem. 18 (1984) 397–406.
[32] M.T. Carter, M. Rodriguex, A.J. Bard, J. Am. Chem. Soc. 111 (1989) 8901–8911.
[33] a) M.J. Waring, J. Mol. Biol. 13 (1965) 269–282;
b) J.K. Barton, J.J. Dannenberg, A.L. Raphael, J. Am. Chem. Soc. 106 (1984) 2172–2176.
[34] J. Carmichael, W.G. DeGraff, A.F. Gazdar, J.D. Minna, J.B. Mitchell, Cancer Res. 47 (1987) 936–942.
[35] A. Gohel, M.B. McCarthy, G. Gronowicz, Endocrinology 140 (1999) 5339–5347.
[36] K.V.P. Chandramohan, P. Gunasekaran, E. Varalakshmi, Y. Hara, S. Nagini, Cell Biol. Int. 31 (2007) 599–608.